

Soft mechanochemical synthesis and thermal stability of hydroxyapatites with different types of substitution

Natalya V. Eremina ^{a*} , Svetlana V. Makarova ^a , Denis D. Isaev ^{ab} ,
Natalia V. Bulina ^a 

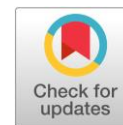
a: Institute of Solid State Chemistry and Mechanochemistry, Siberian Branch of Russian Academy of Sciences, Novosibirsk 630090, Russia

b: Novosibirsk State University, Novosibirsk 630128, Russia

* Corresponding author: eremina@solid.nsc.ru

This paper belongs to the CTFM'22 Special Issue: <https://www.kaznu.kz/en/25415/page>.
Guest Editors: Prof. N. Uvarov and Prof. E. Aubakirov.

© 2022, the Authors. This article is published in open access under the terms and conditions of the Creative Commons Attribution (CC BY) license (<http://creativecommons.org/licenses/by/4.0/>).



Abstract

The feasibility of soft mechanochemical synthesis was studied here for hydroxyapatite with various types of substitution. It was shown that this method allows obtaining hydroxyapatites substituted with copper or iron cations and hydroxyapatites cosubstituted with zinc cations and silicate groups. Thermal stability of the synthesized samples was evaluated. It was found that to preserve phase homogeneity of the material, the temperature during the preparation of ceramic products and coatings should not exceed 600–800 °C. An exception is the hydroxyapatite where a hydroxyl group is expected to be replaced by a copper cation during the synthesis at a degree of substitution $x = 0.5$. For this sample, the temperature of the the heat treatment can be increased to 1100–1200 °C because copper cations return to the hydroxyapatite crystal lattice at these temperatures, and the material becomes single-phase.

Keywords

mechanochemical synthesis
hydroxyapatite
substitution
iron
copper
zinc
silicate
thermal stability

Received: 23.06.22

Revised: 18.07.22

Accepted: 18.07.22

Available online: 26.07.22

1. Introduction

Hydroxyapatite (HA) is an inorganic material of chemical composition $\text{Ca}_{10}(\text{PO}_4)_6(\text{OH})_2$ which crystallizes in hexagonal syngony with a $\text{P6}_3/\text{m}$ space group [1]. The HA unit cell contains 10 calcium cations located at two nonequivalent positions: four cations at the Ca1 site and six cations at the Ca2 site, which are surrounded by nine and seven oxygen ions, respectively. In addition to calcium ions, the HA unit cell contains six phosphate and two hydroxyl groups. The latter are located on the c axis in a hexagonal channel formed by calcium ions and by oxygen ions from phosphate tetrahedrons.

HA is widely used in various fields of medicine and is a suitable material for the construction of biocompatible ceramic products, composites, bone defect fillers, medical cements, and implant coatings [2–4]. Methods are being developed for 3D printing of custom implants, where HA serves as either an additive or a base material from which a product is created [5, 6]. Prospective applications include drug delivery and tissue engineering because HAs appear to be promising carriers of growth factors, bioactive peptides, and various types of cells [7].

In the crystal lattice of HA, all ions can be substituted with isovalent or heterovalent ions of other chemical elements or their chemical groups [8]. Stoichiometric HA has a low resorption rate, which is a disadvantage of bioresorbable materials based on this substance [9]. In addition, stoichiometric HA does not have antibacterial properties. Nonetheless, the introduction of substituent ions into this material can substantially improve required characteristics. For example, doping of HA with copper, iron, zinc, or silver ions can give antibacterial properties to HA-based materials and thereby can prevent inflammation and stimulate new bone growth, which is important for surgical applications [10]. Silicon ions decrease the crystallinity of the material and increase osseointegration and biocompatibility [11, 12]. HA doped with iron ions has magnetic properties used in biomedicine for heating mediators in cancer hyperthermia therapy and in contrast agents for magnetic resonance imaging [13].

Thermal stability of synthetic HA is crucial for the manufacture of ceramics and HA coatings. It is necessary to correctly select the conditions of thermal treatment when a technological process is designed because when substituted HAs are heated, structural transformations can take place,

accompanied by the formation of impurity phases [14, 15], which affect not only physical but also biological properties of the resultant product.

The purpose of this work was to investigate the feasibility of soft mechanochemical synthesis of HA containing different substituents (Fe, Cu, or Zn simultaneously with Si) and to assess thermal stability of the obtained materials.

2. Experimental

Samples of HA with various substituents were prepared via soft mechanochemical synthesis in an AGO-2 planetary ball mill (Russia). A detailed description of the synthesis conditions is provided in ref. [16]. Previously, it was reported that dopants complicate mechanochemical synthesis [17]; as a consequence, the duration of synthesis of substituted HAS was 40 min, whereas that of unsubstituted HA was 30 min.

Expected reactions of mechanochemical synthesis are presented in Table 1. Reagents had purity grade not lower than “chemically pure.” Reaction 1 was expected to generate unsubstituted HA. In reactions 2, 3, 5 and 6, some calcium cations are substituted with either copper or iron cations, whereas in reactions 4 and 7, hydroxyl groups are replaced.

To obtain Cu-substituted HA and Fe-substituted HA, the synthesis was carried out using either an oxide form (reactions 3–5) or a phosphate form of the substituent ion (reactions 2, 6, and 7). Reactions 8 and 9 imply the cosubstitution of calcium cations by zinc cations and of the phosphate group by the silicate group.

Sintering of the powders was conducted in a high-temperature electrical furnace PVK-1.4 at different temperatures for 2 h at heating and cooling rates of 5 °C/min in ambient air.

Powder X-ray diffraction (PXRD) patterns of the samples were recorded on a D8 Advance powder diffractometer (Bruker, Germany) in Bragg–Brentano geometry with Cu K α radiation. For the *in situ* PXRD analysis, a high-temperature chamber HTK 1200N (Anton Paar, Austria) was employed. A sample was heated stepwise in a corundum carrier in ambient air at a heating rate of 12 °C/min. When a required temperature was reached, the heating was stopped, and the

PXRD pattern was registered. X-ray phase analysis of the compounds was performed using a database of PXRD patterns, ICDD PDF-2. Unit cell parameters, crystallite size, and concentrations of crystal phases were determined by the Rietveld method implemented in the Topas 4.2 software (Bruker, Germany). The instrumental contribution was taken into account by the fundamental parameter method.

Fourier transform infrared (FTIR) spectra were acquired with the help of an Infracalum-801 spectrometer (Simex, Russia). The samples were prepared by the KBr pellet method.

3. Results and Discussion

3.1. Mechanochemical synthesis

3.1.1. Cu-substituted HA

Figure 1a shows that PXRD patterns of HA samples containing copper are identical and match the pattern of unsubstituted HA. The observed reflections belong to the HA phase (card PDF 40-11-9308), indicating that the obtained samples are single-phase. The absence of any reflections of impurity phases suggests that the synthesis procedures produced expected substances in accordance with the expected reactions (Table 1). It is obvious that when either the oxide form or the phosphate form of a substituent ion is used, initial reagents are not detectable among the products; therefore, any of the reagents tested here can be utilized for the synthesis of Cu-substituted HA. Infrared spectra of all synthesized samples (Figure 1b) show absorption bands corresponding to the HA structure.

There are bands of the phosphate ion (572, 602, 960, 1048, and 1089 cm⁻¹), OH group (630 and 3573 cm⁻¹), and of carbonate group (CO₃)²⁻ (1420 and 1470 cm⁻¹); the latter came from ambient air during the mechanochemical synthesis. It should be noted that the intensity of the absorption bands of the hydroxyl group is identical between the samples obtained via reactions 3 and 4, although judging by the reactions given in Table 1, the concentrations of the hydroxyl group should differ by a factor of 2. Therefore, in the sample 0.5Cu(O)–OH, copper ions do not replace hydroxyl groups.

Table 1 Expected reactions of mechanochemical synthesis (MCS).

Number	Equations for the expected chemical reaction	Sample name
1	$6\text{CaHPO}_4 + 4\text{CaO} \xrightarrow{\text{MCS}} \text{Ca}_{10}(\text{PO}_4)_6(\text{OH})_2 + 2\text{H}_2\text{O}$	0.0HA
2	$5.5\text{CaHPO}_4 + 4\text{CaO} + 0.5\text{Cu}(\text{HPO}_4)\text{H}_2\text{O} \xrightarrow{\text{MCS}} \text{Ca}_{9.5}\text{Cu}_{0.5}(\text{PO}_4)_6(\text{OH})_2 + n\text{H}_2\text{O}$	0.5Cu(P)–Ca
3	$6\text{CaHPO}_4 + 3.5\text{CaO} + 0.5\text{CuO} \xrightarrow{\text{MCS}} \text{Ca}_{9.5}\text{Cu}_{0.5}(\text{PO}_4)_6(\text{OH})_2 + n\text{H}_2\text{O}$	0.5Cu(O)–Ca
4	$6\text{CaHPO}_4 + 4\text{CaO} + 0.5\text{CuO} \xrightarrow{\text{MCS}} \text{Ca}_{10}(\text{PO}_4)_6(\text{OH})_1\text{Cu}_{0.5}\text{O} + n\text{H}_2\text{O}$	0.5Cu(O)–OH
5	$6\text{CaHPO}_4 + 3.5\text{CaO} + 0.25\text{Fe}_2\text{O}_3 \xrightarrow{\text{MCS}} \text{Ca}_{9.5}\text{Fe}_{0.5}(\text{PO}_4)_6(\text{OH})_{1.5}\text{O}_{0.5} + n\text{H}_2\text{O}$	0.5Fe(O)–Ca
6	$5.334\text{CaHPO}_4 + 3.666\text{CaO} + 0.333\text{Fe}_3(\text{PO}_4)_2 \cdot 8\text{H}_2\text{O} \xrightarrow{\text{MCS}} \text{Ca}_9\text{Fe}_1(\text{PO}_4)_6(\text{OH})_2 + n\text{H}_2\text{O}$	1.0Fe(P)–Ca
7	$5.67\text{CaHPO}_4 + 4.33\text{CaO} + 0.166\text{Fe}_3(\text{PO}_4)_2 \cdot 8\text{H}_2\text{O} \xrightarrow{\text{MCS}} \text{Ca}_{10}(\text{PO}_4)_6(\text{OH})_1\text{Fe}_{0.5}\text{O} + n\text{H}_2\text{O}$	0.5Fe(P)–OH
8	$4.4\text{CaO} + 5.4\text{CaHPO}_4 + 0.2\text{SiO}_2 \cdot n\text{H}_2\text{O} + 0.2\text{Zn}(\text{H}_2\text{PO}_4)_2 \cdot 2\text{H}_2\text{O} \xrightarrow{\text{MCS}} \text{Ca}_{9.8}\text{Zn}_{0.2}(\text{PO}_4)_{5.8}(\text{SiO}_4)_{0.2}(\text{OH})_{1.8} + n\text{H}_2\text{O}$	0.2Zn0.2Si
9	$6\text{CaO} + 3\text{CaHPO}_4 + 1\text{SiO}_2 \cdot n\text{H}_2\text{O} + 1\text{Zn}(\text{H}_2\text{PO}_4)_2 \cdot 2\text{H}_2\text{O} \xrightarrow{\text{MCS}} \text{Ca}_9\text{Zn}_1(\text{PO}_4)_5(\text{SiO}_4)_1(\text{OH})_1 + n\text{H}_2\text{O}$	1.0Zn1.0Si

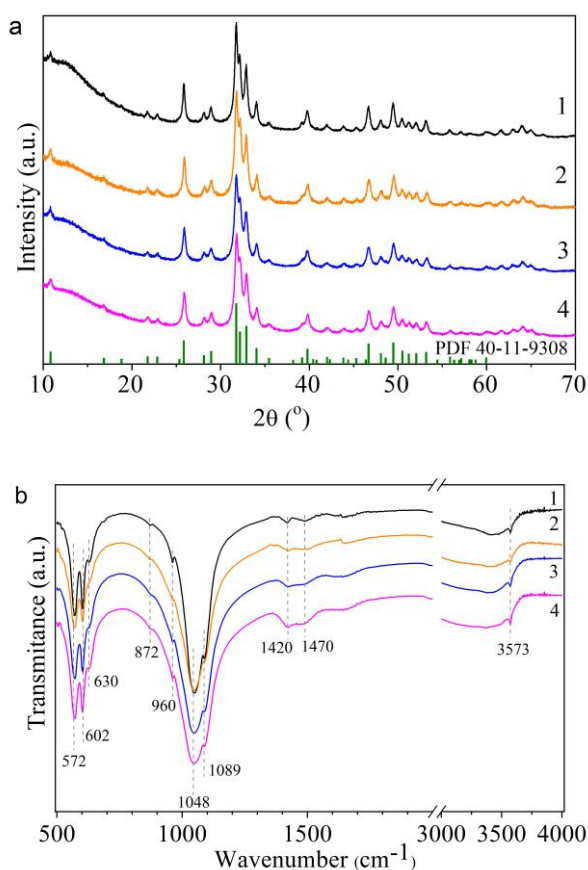


Figure 1 XRD patterns (a) and FTIR spectra (b) of as-synthesized samples 0.0HA (1), 0.5Cu(P)-Ca (2), 0.5Cu(O)-Ca (3), and 0.5Cu(O)-OH (4) according to the (1) – (4) reactions.

Table 2 Structural characteristics of the HA phase in the synthesized samples.

Sample name	a (Å)	c (Å)	Crystallite size (nm)
0.0HA	9.437(1)	6.892(1)	24.9(2)
0.5Cu(P)-Ca	9.431(2)	6.879(1)	20.4(2)
0.5Cu(O)-Ca	9.435(1)	6.881(1)	20.2(2)
0.5Cu(O)-OH	9.432(2)	6.887(1)	20.2(2)
1.0Fe(P)-Ca	9.436(2)	6.877(1)	20.3(2)
0.5Fe(P)-OH	9.435(2)	6.886(1)	20.7(2)
0.2Zn0.2Si	9.435(1)	6.889(1)	20.9(2)
1.0Zn1.0Si	9.434(2)	6.891(1)	16.4(3)

Note: The estimated standard deviations of the refined values are in parentheses.

At the same time, the intensity of absorption bands is much higher in the 0.5Cu(O)-OH sample than in the other ones. It can be concluded that in the 0.5Cu(O)-OH sample, copper cations occupy positions of calcium cations, and the shortage of phosphate ions is compensated by the carbonate ion, which can occupy the phosphate group's position. Consequently, in the samples 0.5Cu(O)-OH and 0.5Cu(O)-Ca, copper cations replace calcium cations. A possible stoichiometric formula of the resultant Cu-substituted HA in the sample 0.5Cu(O)-OH can be written as $\text{Ca}_{10-x}\text{Cu}_x(\text{PO}_4)_{6-y}(\text{CO}_3)_y(\text{OH})_{2-y}\text{O}_y$, where $y = x/1.67$.

Crystal lattice parameters of the synthesized Cu-substituted HAs are lower than those of unsubstituted HA (Table 2). The smaller ionic radius of copper as compared to calcium should diminish the lattice parameters, as observed in our case. The slight difference in the parameter *c* between the samples 0.5Cu(O)-Ca and 0.5Cu(O)-OH can be explained by an influence of the carbonate ion. The size of the crystallites decreases with the introduction of the copper cation (Table 2), meaning that the substituent ion complicates the formation of the HA crystal lattice.

Thus, after 30 min of mechanochemical processing of the mixtures in accordance with reactions 2–4, in all cases, the structure of Cu-substituted HA forms with localization of copper ions at the positions of calcium ions. Therefore, the expected substitution of the hydroxyl group with copper cations does not proceed under our conditions of mechanochemical synthesis. For the synthesis of Cu-substituted HA, it is possible to use both copper oxide and copper (II) hydrogen orthophosphate monohydrate.

3.1.2. Fe-substituted HA

In the XRD patterns of the samples synthesized with the introduction of iron (Figure 2a), one can see that the 0.5Fe(O)-Ca sample, which was obtained using iron (III) oxide, contains reflections of Fe_2O_3 , which was employed as the initial reagent, i.e. the source of the iron cation (Figure 2a). In the sample 1.0Fe(P)-Ca, where iron (II) orthophosphate hydrate was chosen as the initial reagent (the iron source), only reflections of HA were detectable, without additional reflections. Therefore, iron (III) oxide does not enter into the mechanochemical reaction forming the Fe-substituted HA. The 1.0Fe(P)-Ca sample turned out to be single-phase even at a dopant concentration two times higher than that in the case of the sample 0.5Fe(O)-Ca. The sample 0.5Fe(P)-OH, where the hydroxyl group was expected to be replaced by iron cations from iron (II) orthophosphate hydrate, also proved to be single-phase.

Table 2 indicates that after the introduction of iron cations in the phosphate form, in all cases, parameter *a* stay almost the same while parameter *c* declines relative to unsubstituted HA.

The FTIR spectra of the samples 1.0Fe(P)-Ca and 0.5Fe(P)-OH (Figure 2b) are similar to the spectra of unsubstituted HA and of Cu-substituted HA. All absorption bands of the HA structure are present. During the mechanochemical synthesis, the substitution of the hydroxyl group during the attempted introduction of iron cations obviously does not proceed either because a more intense absorption band of the carbonate group is visible in the 0.5Fe(P)-OH spectrum.

According to the literature, high-temperature processing of a material at 1100 °C is performed to place copper and iron cations in the hydroxyl channel [18, 19]. In mechanochemical synthesis, such a temperature is unattainable, which is why it is evidently impossible to synthesize HA containing copper and iron cations in the hydroxyl channel.

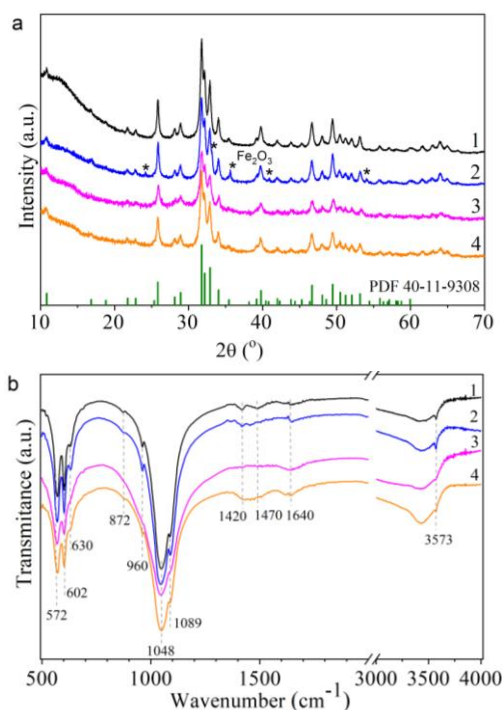


Figure 2 PXR D patterns (a) and FTIR spectra (b) of as-synthesized samples o.oHA (1), 0.5Fe(O)-Ca (2), 1.0Fe(P)-Ca (3), and 0.5Fe(P)-OH (4) according to the (1), (4) – (6) reactions.

3.1.3. Zn-Si-substituted HA

The analysis of the PXR D patterns revealed that after cosubstitution with zinc and silicate the synthesized samples are single-phase (Figure 3a). The lattice parameters of the obtained samples are virtually identical to those of the unsubstituted HA (Table 2). This is probably because the substitution of calcium cations by zinc cations should reduce the lattice parameters owing to a decrease in the ionic radius, while the substitution of the phosphate tetrahedron by the silicate tetrahedron should lead to an increase. After the cosubstitution, the contributions of the substituents cancel each other out.

In the FTIR spectra of the samples 0.2Zn0.2Si and 1.0Zn1.0Si (Figure 3b), there are all absorption bands characteristic of HA. The intensity of hydroxyl bands in the spectra declines with the increasing concentration of the introduced ions, consistently with the equation of the expected reaction (Table 1). In this context, the diminished number of hydroxyl groups is a consequence of compensation of the silicate group's excess negative charge as compared to the phosphate group, which is being replaced.

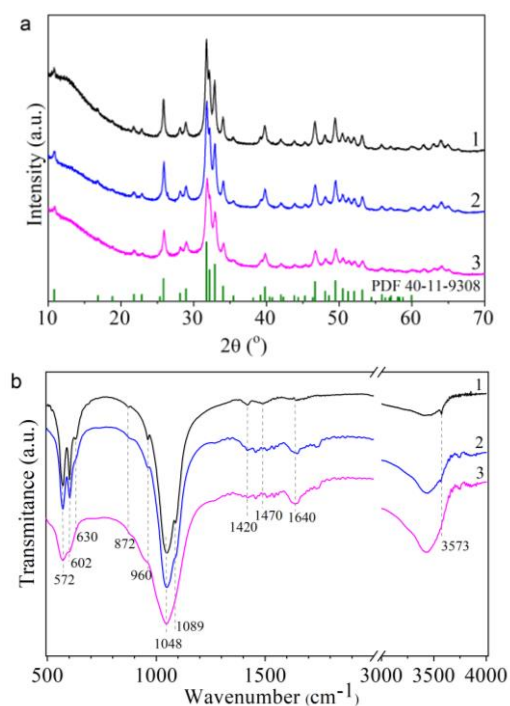


Figure 3 PXR D patterns (a) and FTIR spectra (b) of as-synthesized samples o.oHA (1), 0.2ZnSi (2), and 1.0Zn1.0Si (3) according to the (1), (7) – (8) reactions.

3.2. Thermal stability

3.2.1. Cu-substituted HA

Examination of the synthesized samples by high-temperature *in situ* diffractometry (Figure 4) showed that these samples differ in thermal stability. As illustrated in Figure 4a, the unsubstituted HA is stable up to 1200 °C. Raising the temperature of the thermal treatment enhances the intensity of the reflections and decreases their half-width, thereby indicating the growth of crystallites during the sample heating. There are no reflections of impurity phases in the patterns.

As for the 0.5Cu(O)-Ca sample, in which the dopant was expected to replace calcium ions, its thermal stability is much lower as compared to the unsubstituted HA. Already at 700 °C, copper (II) oxide separates, which is present in the sample up to 1000 °C (Figure 4b, Table 3).

A further increase in temperature causes the CuO reflections to disappear from the diffraction pattern.

Table 3 Concentrations of impurity phases in substituted-HA samples in the *in situ* experiment, as evidenced by diffraction patterns processed by the Rietveld method.

Sample name	Impurity phase (wt.%)	Temperature (°C)							
		500	600	700	800	900	1000	1100	1200
0.5Cu(O)-Ca	β -Ca ₃ (PO ₄) ₂	-	-	-	17	26	27	31	34
	CuO	-	-	1	2	2	1	-	-
0.5Cu(O)-OH	CuO	-	3	4	4	4	3	-	-
1.0Fe(P)-Ca	β -Ca ₃ (PO ₄) ₂	-	-	-	36	57	71	72	74
	Fe ₂ O ₃	-	-	-	1	4	6	7	7
	Fe ₃ O ₄	-	-	-	2	3	2	2	2
0.5Fe(P)-OH	Fe ₂ O ₃	-	-	-	-	1	2	2	-
	Fe ₃ O ₄	-	-	-	2	2	2	2	1

Therefore, there is a reverse process at 1000 °C, namely, diffusion of copper ions into the hydroxyl channel of HA. Additionally, at 800 °C, a large amount of another impurity phase, β - $\text{Ca}_3(\text{PO}_4)_2$, emerges, whose concentration goes up with temperature.

In the 0.5Cu(O)-OH sample, the release of copper oxide starts at a lower temperature - 600 °C. At 1100 and 1200 °C, CuO reflections are absent, and the sample becomes single-phase. It is known that prolonged annealing at 1100 °C of a mixture of reagents containing CuO gives rise to HA containing linear oxocuprate groups in the hydroxyl channel [18, 20]. Accordingly, it is likely that at 1100 °C, copper ions of the 0.5Cu(O)-Ca sample localize to the hydroxide channel, thus yielding the $\text{Ca}_{10}(\text{PO}_4)_6(\text{OH})_{2-2x}\text{Cu}_x\text{O}_{2x}$ structure, and the sample goes back to being single-phase (Figure 4b, Table 3).

Thus, the sample 0.5Cu(O)-Ca is thermally stable up to 700 °C. Stability of 0.5Cu(O)-OH is lower by 200 °C, but at 1100 °C, the newly formed copper (II) oxide phase disappears making the material single-phase again.

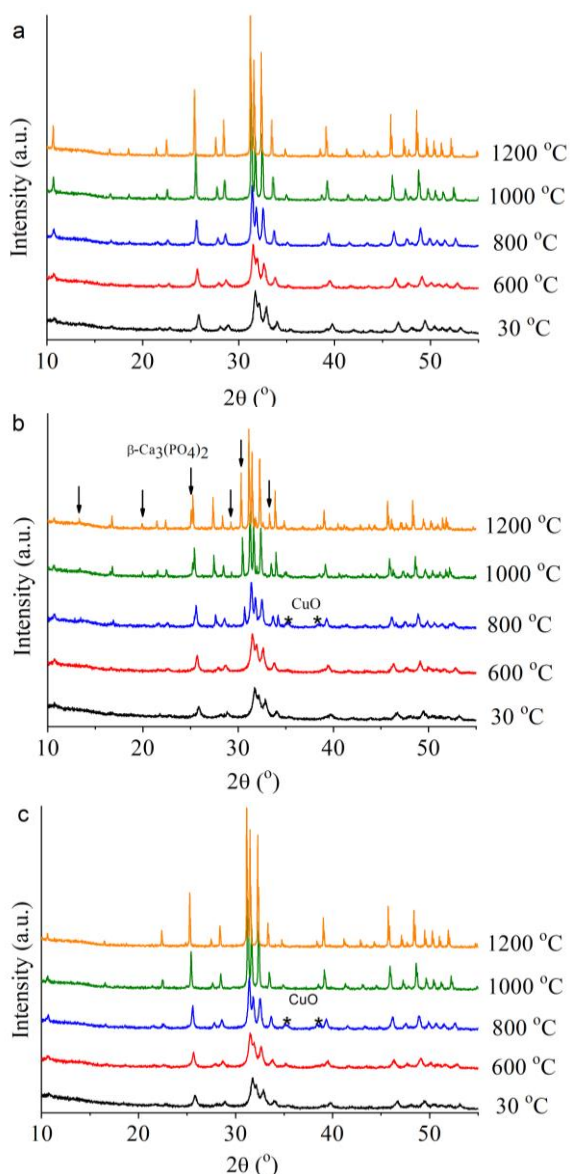


Figure 4 *In situ* high-temperature PXRD patterns of samples 0.0HA (a), 0.5Cu(O)-Ca (b), and 0.5Cu(O)-OH (c).

3.2.2. Fe-substituted HA

In the diffraction pattern of the 1.0Fe(P)-Ca sample, reflections of $\text{Ca}_3(\text{PO}_4)_2$ and Fe_2O_3 phases are clearly visible. Modeling of the diffraction patterns by the Rietveld method detected reflections of the Fe_3O_4 phase as well (Table 3). Judging by these data, thermal stability of the materials containing iron cations (samples 1.0Fe(P)-Ca (a) and 0.5Fe(P)-OH) is equally low. The introduced cation is released in the oxide form starting at a temperature of 800 °C in both cases (Table 3). The sum of concentrations of the oxide phases is approximately twofold for the 1.0Fe(P)-Ca sample than for 0.5Fe(P)-OH because the concentration of introduced iron is 2 times higher in the former case than in the latter. The concentration of β - $\text{Ca}_3(\text{PO}_4)_2$ seen in the 1.0Fe(P)-Ca sample increases with temperature, reaching a maximum at 1200 °C (Figure 5a, Table 3).

In contrast to the doping with copper cations, in the samples with iron cations, there is no complete disappearance of the substituent ion during the high-temperature treatment. Perhaps the reason is lower solubility of iron in HA.

Thus, we can assume that the samples 1.0Fe(P)-Ca and 0.5Fe(P)-OH are thermally stable up to 800 °C.

3.2.3. Zn-Si-substituted HA

After the cosubstitution with zinc cations and silicate groups, the material also has lower thermal stability than the unsubstituted HA.

In the PXRD patterns of the sample 0.2Zn0.2Si at 1000 °C, reflections of additional phases come into being, such as ZnO and β - $\text{Ca}_3(\text{PO}_4)_2$ (Figure 6a). In the 1.0Zn1.0Si sample, ZnO reflections appear already at 800 °C, but the β - $\text{Ca}_3(\text{PO}_4)_2$ phase still forms at 1000 °C (Figure 6b).

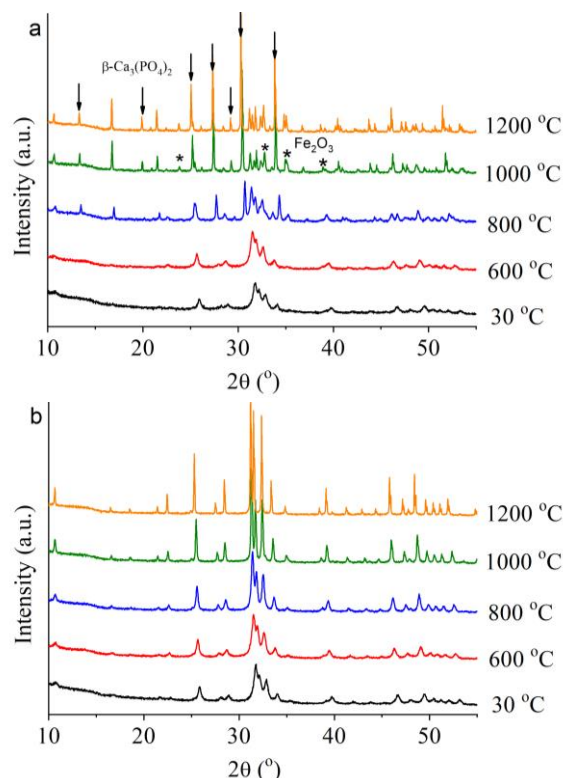


Figure 5 *In situ* high-temperature PXRD patterns of samples 1.0Fe(P)-Ca (a) and 0.5Fe(P)-OH (b).

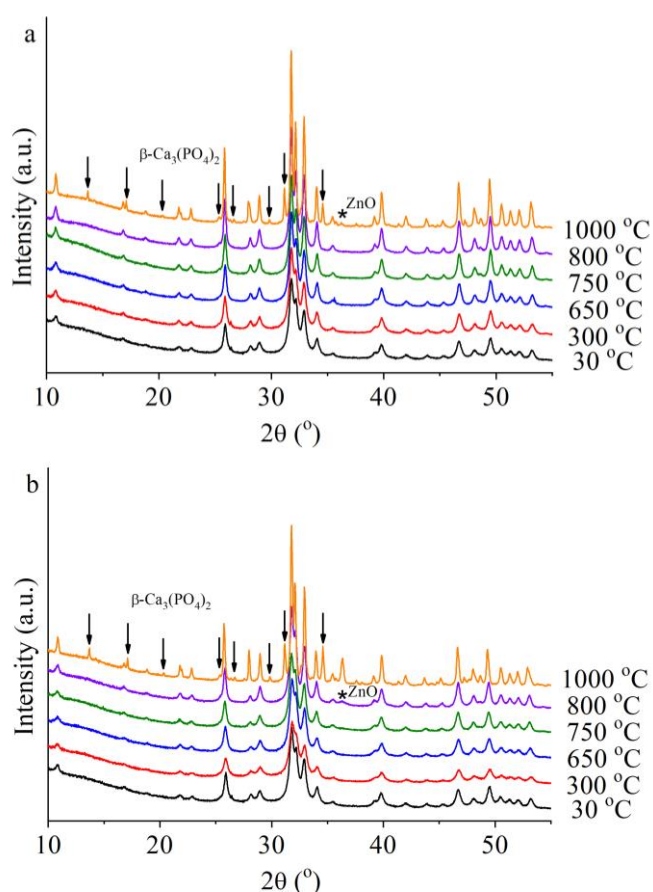


Figure 6 PXRD patterns of samples 0.2Zn0.2Si (a) and 1.0Zn1.0Si (b) after heating.

Therefore, thermal stability of cosubstituted Zn-Si-HA depends on concentrations of the substituent ions. The higher their concentrations, the lower is the stability of the material. Obviously, during the thermal treatment, zinc cations leaving their positions (previously belonging calcium ions) create vacancies at the former calcium positions. A large number of such vacancies promotes structural transformations, which generate the β - $\text{Ca}_3(\text{PO}_4)_2$ and ZnO phases.

4. Conclusions

It was demonstrated that Cu-substituted HA and Fe-substituted HA can be synthesized mechanochemically via the introduction of the dopants at calcium positions. For the synthesis of such materials, 40 min is sufficient when an appropriate mixture of initial reagents is mechanochemically processed in a planetary ball mill. It was shown that for the synthesis of Cu-substituted HA, either copper (II) oxide or copper (II) hydrogen orthophosphate monohydrate can be utilized as a reagent providing the substituent ion. As for the synthesis of Fe-substituted HA, the stablest oxide of the substituent (Fe_2O_3) is not suitable, but iron (II) orthophosphate hydrate is suitable. The mechanochemical method also allows to synthesize HA with cosubstitution of calcium cations by zinc and of phosphate tetrahedra by silicate ones. For this synthesis, silicic acid, and zinc (II) dihydrogen phosphate hydrate can be used.

Thermal stability of the obtained substituted HAs is significantly lower than that of the stoichiometric unsubstituted HA. At 600–800 °C, in the substituted-HA samples containing copper, iron, or zinc at the position of calcium ions with a degree of substitution (x) of ≥ 0.5 , a release of the corresponding oxides is observed, pointing to the diffusion of the substituent ions onto the surface of substituted-HA particles. The created vacancies at calcium ions' positions promote structural transformations, which give rise to the β - $\text{Ca}_3(\text{PO}_4)_2$ phase.

It was demonstrated here that in the HA sample where copper cations are expected to replace the hydroxyl group, a CuO phase emerges during the thermal treatment at 600 °C. On the other hand, a further increase in temperature, to 1100 °C, results in a single-phase material in which copper cations redissolve in the crystal lattice of HA, thereby most likely localizing to the hydroxyl channel.

The observed changes in phase composition of the synthesized samples can significantly affect the properties of the materials. Low thermal stability of the materials imposes limitations on the manufacture of ceramic products or coatings from HA containing such substituents as copper, iron, or zinc ions.

Supplementary materials

No supplementary materials are available.

Funding

The synthesis and analysis of the iron compounds was carried out within a grant from the Russian Science Foundation (No. 21-12-00251). The research on the compounds containing copper, zinc, and silicon was conducted within the framework of a state assignment for the Institute of Solid State Chemistry and Mechanochemistry SB RAS (project No. 121032500064-8).



Acknowledgments

None.

Author contributions

Conceptualization: B.N.V., E.N.V.
 Data curation: M.S.V.
 Funding acquisition: B.N.V.
 Investigation: M.S.V., I.D.D.
 Methodology: B.N.V., E.N.V., M.S.V.
 Project administration: B.N.V.
 Resources: M.S.V., I.D.D.
 Visualization: E.N.V.
 Writing – original draft: E.N.V., M.S.V., I.D.D.
 Writing – review & editing: B.N.V.

Conflict of interest

The authors declare no conflict of interest.

Additional information

Author IDs:

Natalya V. Eremina, Scopus ID [8637401500](#);
Svetlana V. Makarova, Scopus ID [57212079249](#);
Denis D. Isaev, Scopus ID [57316390200](#);
Natalia V. Bulina, Scopus ID [6602885126](#).

Websites:

Institute of Solid State Chemistry and Mechanochemistry, <http://www.solid.nsc.ru>;
Novosibirsk State University, <https://www.nsu.ru>.

References

- Hughes M, Rakovan J. The crystal structure of apatite, $\text{Ca}_5(\text{PO}_4)_3(\text{F},\text{OH},\text{Cl})_2$. *Rev Mineral Geochem.* 2002;48(1):1–12. doi:[10.2138/rmg.2002.48.1](#)
- Dorozhkin SV. Calcium orthophosphates (CaPO_4): occurrence and properties. *Prog Biomater.* 2016;5(1):9–70. doi:[10.1007/s40204-015-0045-z](#)
- Mucalo MR. Hydroxyapatite (HAp) for biomedical applications: Woodhead Publishing Limited Waltham; 2015. 364 p.
- Kenny SM, Buggy M. Bone cements and fillers: a review. *J Mater Sci Mater Med.* 2003;14(11):923–938. doi:[10.1023/A:1026394530192](#)
- Kumar A, Kargozar S, Baino F, Han S. Additive manufacturing methods for producing hydroxyapatite and hydroxyapatite-based composite scaffolds. *A Rev Front Mater.* 2019;6:313. doi:[10.3389/fmats.2019.00313](#)
- Han Y, Wei Q, Chang P, Hu K, Okoro OV, Shavandi A, Nie L. Three-dimensional printing of hydroxyapatite composites for biomedical application. *Cryst.* 2021;11(4):353. doi:[10.3390/cryst11040353](#)
- Mondal S, Dorozhkin SV, Pal U. Mondal S, Dorozhkin SV, Pal U. Recent progress on fabrication and drug delivery applications of nanostructured hydroxyapatite. *WIREs Nanomed Nanobiotechnol.* 2018;10(4):e1504. doi:[10.1002/wnan.1504](#)
- Šupová M. Substituted hydroxyapatites for biomedical applications: a review. *Ceram Int.* 2015;41(8):9203–9231. doi:[10.1016/j.ceramint.2015.03.316](#)
- Dorozhkin SV. Calcium orthophosphates in nature, biology and medicine. *Mater.* 2009;2(2): 399–498. doi:[10.3390/ma2020399](#)
- Kolmas J, Groszyk E, Kwiatkowska-Różycka D. Substituted Hydroxyapatites with Antibacterial Properties. *BioMed Res Int.* 2014;2014:178123. doi:[10.1155/2014/178123](#)
- Patel N, Best SM, Bonifield W, Gibson IR, Hing KA, Damien E, Revell PA. A comparative study on the *in vivo* behavior of hydroxyapatite and silicon substituted hydroxyapatite granules. *J Mater Sci Mater Med.* 2002;13(12):1199–1206. doi:[10.1023/a:1021114710076](#)
- Anwar A, Akbar S, Sadiqa A, Kazmi M. Novel continuous flow synthesis, characterization and antibacterial studies of nanoscale zinc substituted hydroxyapatite bioceramics. *Inorg Chim Acta.* 2016;453:16–22. doi:[10.1016/j.ica.2016.07.041](#)
- Mondal S, Manivasagan P, Bharathiraja S, Moorthy MS, Kim HH, Seo H, Lee KD, Oh J. Magnetic hydroxyapatite: a promising multifunctional platform for nanomedicine application. *Int J Nanomed.* 2017;12:8389–8410. doi:[10.2147/IJN.S147355](#)
- Bulina NV, Chaikina MV, Prosanov IY, Gerasimov KB, Ishchenko AV, Dudina DV. Mechanochemical synthesis of SiO_4^{4-} - substituted hydroxyapatite, part III – thermal stability. *Eur J Inorg Chem.* 2016;2016(12):1866–1874. doi:[10.1002/ejic.201501486](#)
- Othmani M, Bachoua H, Ghandour Y, Aissa A, Debbabi M. Synthesis, characterization and catalytic properties of copper-substituted hydroxyapatite nanocrystals. *Mater Res Bull.* 2018;97:560–566. doi:[10.1016/j.materresbull.2017.09.056](#)
- Chaikina MV, Bulina NV, Vinokurova OB, Prosanov IY, Dudina DV. Interaction of calcium phosphates with calcium oxide or calcium hydroxide during the “soft” mechanochemical synthesis of hydroxyapatite. *Ceram Int.* 2019;45(14):16927–16933. doi:[10.1016/j.ceramint.2019.05.239](#)
- Makarova SV, Bulina NV, Prosanov IY, Chaikina MV, Ishchenko AV. Mechanochemical synthesis of apatite with the simultaneous substitutions of calcium by lanthanum and phosphate by silicate. *Russ J Inorg Chem.* 2020;65(12):1831–1837. doi:[10.1134/S0036023620120116](#)
- Baikie T, Ng GM, Madhavi S, Pramana SS, Blake K, Elcombe M, White TJ. The crystal chemistry of the alkaline-earth apatites $\text{A}_{10}(\text{PO}_4)_6\text{Cu}_x\text{O}_y(\text{H})_z$ (A = Ca, Sr and Ba). *Dalton Trans.* 2009;34: 6722–6726. doi:[10.1039/b906639j](#)
- Gomes S, Kaur A, Nedelec JM, Renaudin G. X-ray absorption spectroscopy shining (synchrotron) light onto the insertion of Zn^{2+} in calcium phosphate ceramics and its influence on their behavior under biological conditions. *J Mater Chem B.* 2014;2(5):536–545. doi:[10.1039/C3TB21397H](#)
- Karpov AS, Nuss J, Jansen M, Kazin PE, Tretyakov YD. Synthesis, crystal structure and properties of calcium and barium hydroxyapatites containing copper ions in hexagonal channels. *Solid State Sci.* 2003;5(9):1277–1283. doi:[10.1016/S1293-2558\(03\)00152-3](#)